Pergamon

0301-9322(94)00038-7

*Int. J. Multiphase Flow* Vol. 20, No. 6, pp. 1039–1052, 1994

0301-9322/94 $7.00 + 0.00

# SPECTRUM OF DENSITY FLUCTUATIONS IN A PARTICLE–FLUID SYSTEM—II. POLYDISPERSE SPHERES

S. SUNDARAM and L. R. COLLINS†

Department of Chemical Engineering, The Pennsylvania State University, University Park, PA 16802, U.S.A.

*(Received 7 September 1993; in revised form 25 April 1994)*

**Abstract**—This paper presents an extension of the analysis shown in Part I to a polydisperse particle–fluid system. The density autocorrelation is shown to be a function of two quantities, a generalized Overlap function for which an analytical expression is derived, and the radial distribution function (RDF). In Fourier transform space, the density spectrum again appears to be a strong function of the mean particle size, and secondarily the mean particle separation distance. One unusual result is previously observed oscillations in the density spectrum of a monodisperse system of particles are severely dampened or even eliminated in the polydisperse case, depending on the width of the particle size distribution. Apparently contributions from different particle correlations interfere with each other, thereby reducing the coherent oscillations seen in the monodisperse particle–fluid system. Furthermore at large wavenumbers, the spectrum decays with a $-2$ power-law, independent of the shape of the particle size distribution. This behavior can be traced to the Overlap function which controls the behavior of the spectrum beyond the first peak. Remarkably the $-2$ power-law spectrum is determined by the shape of the particles (i.e. spheres) rather than their spatial distribution (RDF).

The effect of an asymptotically large pressure gradient on the correlation of several important higher-order moments is revisited for the polydisperse system. The relatively simple relationships developed for the monodisperse system are lost in the polydisperse case because particles of different sizes will be influenced differently by an applied pressure gradient. The result is moments that are of different order in velocity can no longer be related to each other (as they were in the monodisperse system), even in this idealized flow. A more comprehensive understanding of this phenomenon can only be achieved through direct numerical simulation or experiment.

*Key Words:* two-phase flow, turbulence, polydisperse, spectral analysis, density autocorrelation

## INTRODUCTION

In a previous publication (hereafter referred to as Part I), Sundaram & Collins (1994) proposed a methodology for determining spectral statistics of a particle-laden flow based on considering the particle–fluid mixture as a single pseudo-fluid with discontinuities in density at the particle boundaries. Two-point correlations are then perfectly equivalent to those for a single incompressible fluid, with the exception that in this case correlations between the fluid–fluid, particle–fluid, and particle–particle phases must be accounted for. Their analysis led to a simple expression for the density autocorrelation for a monodisperse system of particles. The autocorrelation was found to be a function of two distinct quantities, the Overlap function which is completely defined by the geometry of the particles (spheres in this case), and the radial distribution function (RDF), which depends on the relative location of the particles. The Overlap function, for particles of different sizes, can be derived from simple geometrical considerations by considering the intersection volume of the particles. Percus & Yevick (1958) developed an approximate equation for the RDF of a hard sphere system. An analytical solution of the Percus–Yevick equation, derived by Smith & Henderson (1970), was used to obtain the RDF. One surprising result of the study was the density autocorrelation in Fourier transform space was found to have multiple peaks whose locations scale primarily with the particle size and secondarily with the mean particle separation distance or equivalently the concentration. The qualitative shape of the density spectrum for the particle-laden flow indicates a clear departure from classical spectra for incompressible single-fluid turbulence (Ishii 1975). This paper presents a generalization of the previous study to a polydisperse

†Author to whom all correspondence should be addressed.

mixture of particles. In this case, particle interactions can occur between like and unlike pairs of particles, hence the joint RDFs for all possible combinations are required. The exact solution to the Percus–Yevick approximation for a mixture of hard spheres, first derived by Lebowitz (1964) has been used to determine the RDFs. It is recognized that the PY equation contains no information regarding the influence turbulent fluctuations in the suspending fluid may have on the RDFs, hence the application is again restricted to circumstances where that effect is small (e.g. high concentration of particles, gaseous carrier fluid and very low concentration of particles). Once again we appeal to experimentalists and simulators to measure the RDFs for mixtures of hard spheres in more realistic turbulent flows. The details of the analysis have been presented in Part I, therefore the emphasis in Part II has been placed on describing the effects of polydispersity on the earlier results. The generalized equations for the density autocorrelation in physical space and spectral space have been derived. Furthermore, the case of interpenetration of particles and fluid due to an asymptotically large pressure gradient (e.g. shock wave) is revisited. Previously it was shown that the results for the density autocorrelation could be extended to higher-order volocity correlations (e.g. Reynolds stress) in this limit. The effect polydispersity has on the analysis, and on the higher-order moments (as presented in Part I) will be discussed in detail.

## THE DENSITY AUTOCORRELATION

The density autocorrelation for a homogeneous particle–fluid system is defined as

$$B(\mathbf{r}) = \overline{\rho_1'(\mathbf{x})\rho'(\mathbf{x}+\mathbf{r})} \qquad [1]$$

As shown previously (Part I), the density autocorrelation for monodisperse spheres is related to the $\beta$-correlation, in the following manner

$$B(\mathbf{r}) = \overline{\beta_1'(\mathbf{x})\beta_1'(\mathbf{x}+\mathbf{r})}(\rho_p - \rho_f)^2 \qquad [2]$$

where $\overline{\beta_1'(\mathbf{x})\beta_1'(\mathbf{x}+\mathbf{r})}$ is the $\beta$-correlation (see Part I for definition), $\rho_p$ is the density of the particles and $\rho_f$ is the density of the fluid phase. The analysis in Part I then derived the relationship between the $\beta$-correlation and the Overlap function and RDF. The results are summarized below

$$\overline{\beta_1'(\mathbf{x})\beta_1'(\mathbf{x}+\mathbf{r})} = \frac{\alpha_1}{V_p} I(|\mathbf{r}|) + \left(\frac{\alpha_1}{V_p}\right)^2 \int I(|\mathbf{r}-\mathbf{z}|)h(|\mathbf{z}|)\,d\mathbf{z} \qquad [3]$$

or in transform space

$$\widehat{\overline{\beta_1'\beta_1'}} = \frac{\alpha_1}{V_p} I(k)\left[1 + \frac{\alpha_1}{V_p}\hat{h}(k)\right] \qquad [4]$$

where $\alpha_1$ is the volume fraction of particles, $I(r)$ is the Overlap function, $V_p$ is the volume of a particle and $h(r)$ is the RDF. The superscript $\hat{}$ refers to the three dimensional Fourier transform. Equation [4] shows that the density autocorrelation in transform space can be expressed as a sum of two contributions, the first being a geometric expression that quantifies the particle self-correlation or intra-particle correlation, and the second accounts for the inter-particle correlations between pairs of particles. The second term is related to the distribution of particles in the system which is characterized by the RDF. The analysis for a polydisperse system will proceed in an analogous manner, except that now we must allow for different particle categories based on the particle diameter.

Consider a volume $V$ which contains m different categories of particles, each designated by an index $j$, where $j = 1, \ldots, m$. Particles in all categories are assumed to have a uniform density, $\rho_p$. Particle diameters will be designated by $\sigma_1, \ldots, \sigma_m$, and the number of particles within each category by $N_1, \ldots, N_m$. Once again it will be possible to define a $\beta$-function for each category of particles

$$\beta_j = \begin{cases} 1 & \text{particles of size } \sigma_j \\ 0 & \text{everywhere else} \end{cases}$$

Mathematically,

$$\beta_j(\mathbf{x}) = \sum_{q=1}^{N_j} H\left[\frac{\sigma_j}{2} - |\mathbf{x} - \mathbf{x}_{j_q}|\right] \quad [5]$$

where $\mathbf{x}$ is the position vector, and $\mathbf{x}_{j_q}$ is the location of the $q$th particle of type $j$.

Likewise a $\beta$-function for the fluid is defined by

$$\beta_f = \begin{cases} 1 & \text{within fluid} \\ 0 & \text{everywhere else} \end{cases}$$

$$\beta_f(\mathbf{x}) = 1 - \sum_{j=1}^{m} \beta_j(\mathbf{x}) \quad [6]$$

based on the fact that the sum of the $\beta$-functions is unity. The local microscopic density can then be expressed by

$$\rho(\mathbf{x}) = \rho_f + \sum_{j=1}^{m} (\rho_p - \rho_f)\beta_j(\mathbf{x})$$

Performing an ensemble average (see Part I for definition) then yields

$$\bar{\rho} = \rho_f + (\rho_p - \rho_f) \sum_{j=1}^{m} \alpha_j$$

where $\alpha_j$ is the volume fraction of particles of type $j$. By subtraction, the density fluctuation can be expressed in terms of the $\beta$-correlation in the following manner

$$\rho'(\mathbf{x}) = (\rho_p - \rho_f) \sum_{j=1}^{m} \beta_j'(\mathbf{x}) \quad [7]$$

which is a straightforward generalization of the result found in Part I. Substituting [7] into [1] yields

$$B(\mathbf{r}) = (\rho_p - \rho_f)^2 \sum_{j=1}^{m} \sum_{i=1}^{m} \beta_{ij}(\mathbf{r}) \quad [8]$$

where

$$\beta_{ij}(\mathbf{r}) \equiv \overline{\beta_i'(\mathbf{x})\beta_j'(\mathbf{x}+\mathbf{r})}$$

is a general representation of correlations between like ($i = j$) and unlike ($i \neq j$) pairs of particles. Transforming [8] results in

$$\hat{B}(\mathbf{k}) = (\rho_p - \rho_f)^2 \sum_{j=1}^{m} \sum_{i=1}^{m} \hat{\beta}_{ij}(\mathbf{k}) \quad [9]$$

The relationships for the more generalized $\beta$-correlations shown in [8] and [9] can be related to the RDFs by following the same procedure discussed in Part I for a monodisperse system. The resulting expressions in physical space and transform space are respectively

$$\hat{\beta}_{ij}(\mathbf{r}) = \frac{\alpha_i}{V_{pi}} \delta_{ij} I_{ij}(|\mathbf{r}|) + \frac{\alpha_i}{V_{pi}} \frac{\alpha_j}{V_{pj}} \int I_{ij}(|\mathbf{r} - \mathbf{z}|) h_{ij}(|\mathbf{z}|)\, d\mathbf{z}$$

$$\hat{\beta}_{ij}(\mathbf{k}) = \frac{\alpha_i}{V_{pi}} \hat{I}_{ij}(k)\left[\delta_{ij} + \frac{\alpha_j}{V_{pj}} \hat{h}_{ij}(k)\right] \quad [10]$$

where $h_{ij}$ and $\hat{h}_{ij}$ are the cross RDF for particles of type $i$ and $j$ in physical and transform space respectively and $\delta_{ij}$ is the Dirac delta function. Repeated indices do not imply summation unless otherwise specified. It should be noted that intra-particle contributions are limited to like correlations only ($i = j$) by definition. Equation [10] shows the relationship between the more generalized $\beta$-correlations and the Overlap function and RDF. The generalized 3-dimensional Overlap function $I_{ij}(y)$ is defined as the volume of intersection between two spheres of diameters $\sigma_i$ and $\sigma_j$, respectively, whose centers are separated by a distance $y$. This volume is depicted

schematically in figure 1. From consideration of the volumes of rotation for each sphere, the Overlap function in three dimensions can be shown to be

$$I_{ij}(y) = \begin{cases} \dfrac{\pi\sigma_i^3}{6} & 0 \leqslant y \leqslant \lambda \\ \dfrac{\pi}{6}\left(\dfrac{\sigma_i^3}{2} + \dfrac{\sigma_j^3}{2} - \dfrac{3(\sigma_i^2 y_i + \sigma_j^2 y_j)}{2} + 2(y_i^3 + y_j^3)\right) & \lambda \leqslant y \leqslant \sigma_{ij} \\ 0 & y \geqslant \sigma_{ij} \end{cases} \quad [11]$$

where

$$\lambda = \frac{\sigma_j - \sigma_i}{2}, \quad \sigma_{ij} = \frac{\sigma_j + \sigma_i}{2}, \quad y_i = \frac{y}{2} - \frac{\sigma_j^2 - \sigma_i^2}{8y}$$

and

$$y_j = \frac{y}{2} + \frac{\sigma_j^2 - \sigma_i^2}{8y}.$$

For the sake of convention we assume $\sigma_j \geqslant \sigma_i$. It should be noted that the like Overlap function, recovered by setting $i = j$, reduces to the expression derived in Part I. The Fourier transform of the Overlap function is then given by

$$\hat{I}_{ij}(k) = 4\pi^2 \frac{\left(k\sigma_i \cos\frac{k\sigma_i}{2} - 2\sin\frac{k\sigma_i}{2}\right)\left(k\sigma_j \cos\frac{k\sigma_j}{2} - 2\sin\frac{k\sigma_j}{2}\right)}{k^6} \quad [12]$$

The transform has units of volume$^2$ or length$^6$.

The radial distribution function for a polydisperse system of hard spheres is obtained using the exact solution of the Percus–Yevick equation for a system of hard spheres originally derived by Lebowitz (1964).

## RESULTS AND DISCUSSION

Before calculating the density autocorrelation for a polydisperse system, we decided to examine a binary system of hard spheres. Figure 2(a) details the transition of the density autocorrelation as we go from a monodisperse system 1 ($\sigma_1 = 1$) to monodisperse system 2 ($\sigma_2 = 2$) while maintaining the total particle density ($\alpha_1 + \alpha_2$) constant, which translates to maintaining a constant area under the $B(k)$ curves. The concentration of $A$ particles of diameter unity is decreased from

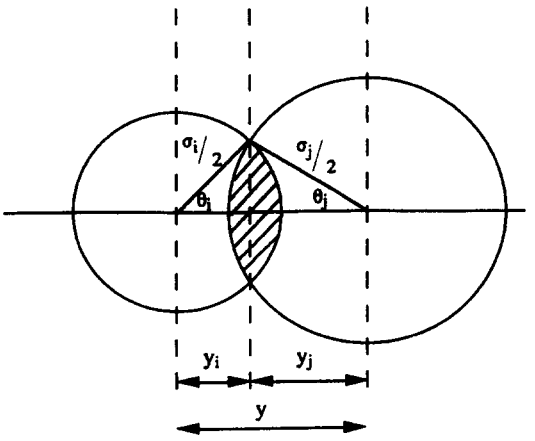


Figure 1. Schematic of the intersecting volume between two overlapping spheres of diameters $\sigma_i$ and $\sigma_j$, respectively. The overlap function, $I_{ij}(y)$ is by definition proportional to the volume of intersection (cross-hatched volume).

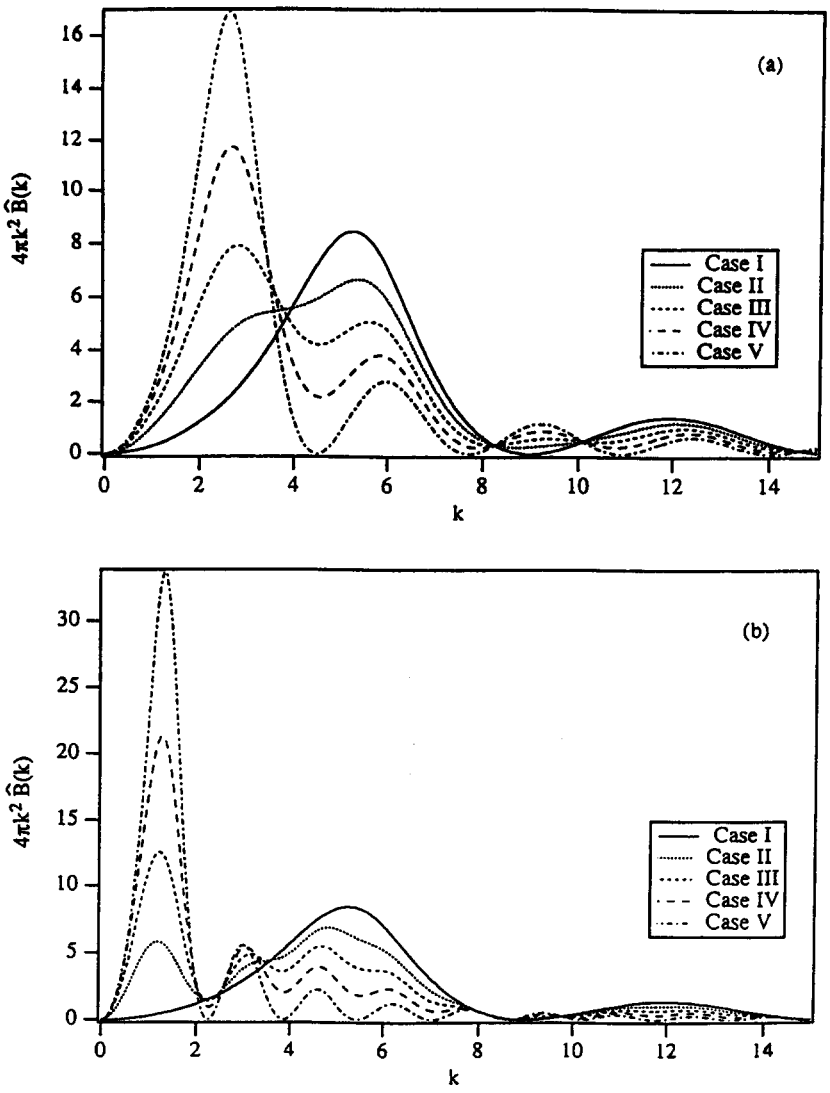


Figure 2. Density autocorrelation for a binary system of particles with diameter ratios of (a) 2 and (b) 4. The total particle concentration was maintained at 0.20 while the concentration of the larger particles was 0.00 (case I), 0.05 (Case II), 0.10 (Case III), 0.15 (Case IV) and 0.20 (Case V).

0.2 to 0.0 by steps of 0.05 over the five cases, while the concentration of the *B* particles is increased from 0 to 0.2, maintaining a constant total particle concentration of 0.2. In the monodisperse limits, the present results agree with the results presented in Part I. It should be noted that the current plots are strictly dimensional because of the ambiguity associated with determining a length scale in a polydisperse system. As pointed out in Part I, the location of the first maximum in the Fourier space autocorrelation plots is related to the mean separation distance which, in turn, scales with the particle size for moderate concentrations. However for mixtures, the twin maxima in the transition region correspond to the now two identifiable length scales (the two particle sizes). Figure 2(b) shows the equivalent calculation for a binary system with a diameter ratio of four. These results are qualitatively the same as in the previous case, the larger ratio serving only as a scaling factor.

Next we consider a truly polydisperse system, with a Gaussian particle size distribution. The mean particle size and variance of the distribution were varied to study the influence of the range of particle sizes on the density autocorrelation. Figure 3(a) shows the three Gaussian particle size distributions we selected, each with a mean particle diameter of unity and standard deviations that lie between 0.15 and 0.25. Case I corresponds to a standard deviation of 0.15, Case II—0.20 and Case III—0.25. The calculated density autocorrelation for these three cases are shown in linear and

logarithmic co-ordinates in figures 3(b) and 3(c) respectively. As expected the narrow range Gaussian is closest to the monodisperse case. With increasing width of size distributions (increasing polydispersity) we find that the oscillations in the spectrum are increasingly dampened out, until finally in Case III they are completely removed. An explanation for the dampening of the oscillations with increasing spread in the distribution can be found by first re-considering the monodisperse system. As shown in Part I the spectrum for the density autocorrelation showed the surprising result of multiple peaks, with a wavelength that scaled with the particle separation distance at small $k$ and with the particle size at large $k$. To a first approximation, the polydisperse system is a superposition of many monodisperse curves, each oscillating with a wavelength that corresponds to its particular size. These curves have phases that interfere with each other hence the superposition reduces or even eliminates the oscillations, if the polydispersity is sufficient. For example, Case III in figure 3(b) is a smooth monotonic curve. Figure 3(c) shows logarithmic plots of the density autocorrelation for each of the different cases. It is interesting to note that the large $k$ behavior in all three curves is a $-2$ power-law spectrum that begins essentially immediately

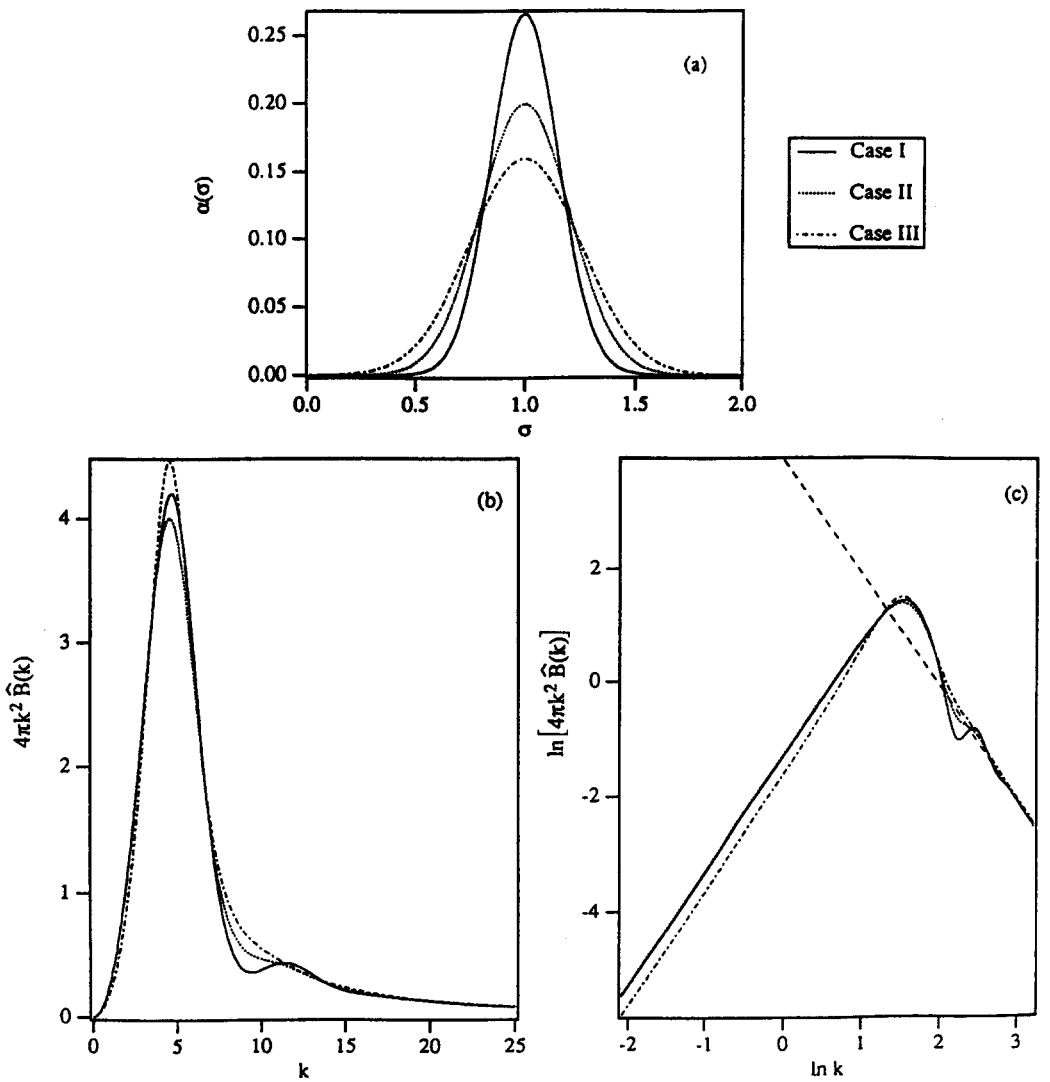


Figure 3. Density autocorrelation for a polydisperse particle-fluid system. The particle size distribution was assumed Gaussian with a mean particle diameter of unity and standard deviations of 0.15 (Case I), 0.20 (Case II) and 0.25 (Case III). Total particle concentration is maintained at 0.10. (a) Shows the particle size distributions, (b) shows the density autocorrelation in linear co-ordinates and (c) shows the same in logarithmic co-ordinates. The dashed line indicates a line of slope $-2$.

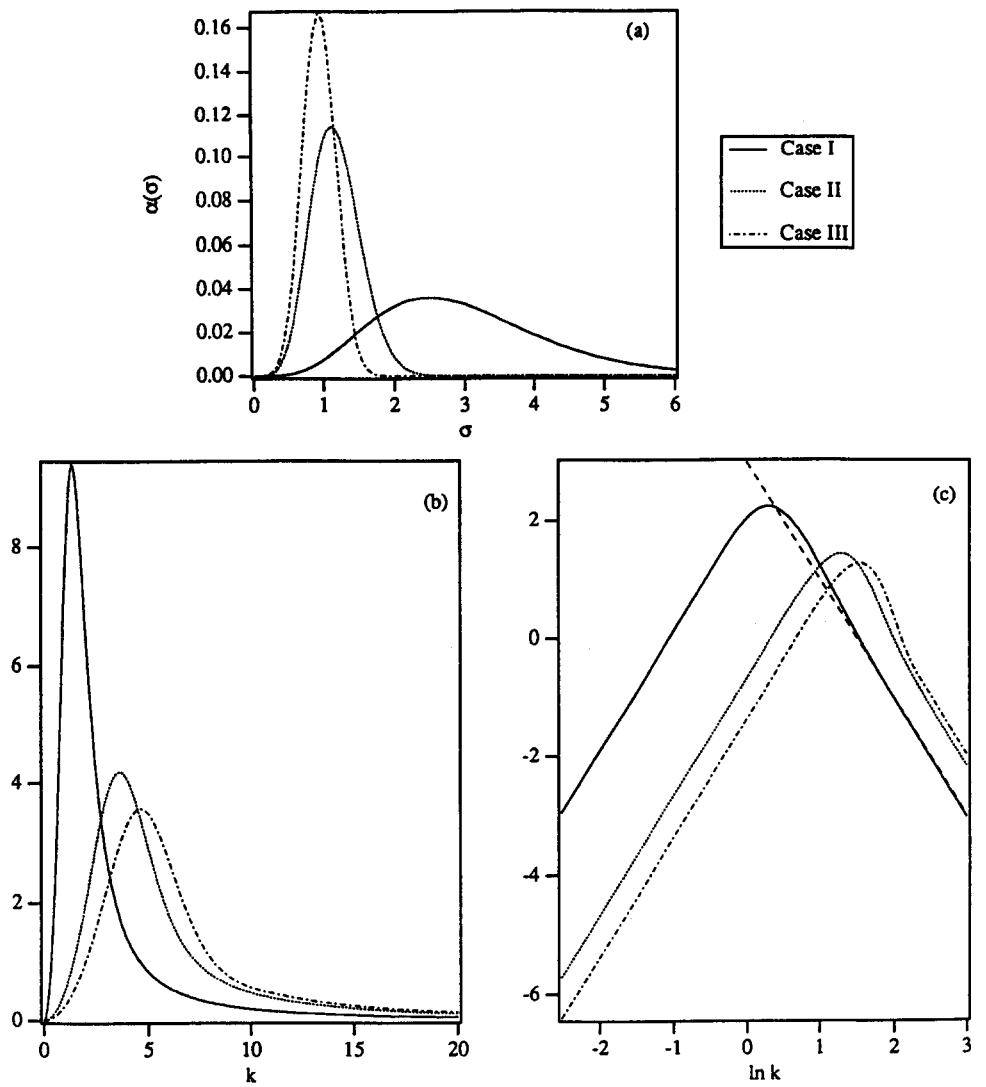


Figure 4. A comparison of particle size distributions with opposing tails. The distributions were calculated from [7] with $c_1 = 5$, $c_2 = 2$, $c_3 = 1$ (Case I), $c_1 = 5$, $c_2 = 2$, $c_3 = 2$ (Case II), $c_1 = 5$, $c_2 = 2$, $c_3 = 3$ (Case III). Total particle concentration is maintained at 0.10. (a) Shows the particle size distributions, (b) shows the density autocorrelation in linear co-ordinates and (c) shows the same in logarithmic co-ordinates. The dashed line indicates a line slope $-2$.

following the maximum in the curve. This large $k$ limit appears to be independent of the spread in the Gaussian distribution. We shall momentarily defer discussing the $-2$ spectrum while we consider the effect of asymmetry in the particle size distribution.

To study the influence of the exact nature of the particle size distribution itself on the autocorrelation, we employed a generic function of the form

$$\alpha(\sigma_i) = \sigma_i^{c_1} e^{-c_2 \sigma_i^{c_3}} \qquad [7]$$

Different tails (degrees of asymmetry) for the particle size distribution are obtained by varying the parameter $c_3$ ($c_1 = 5$ and $c_2 = 2$ throughout). The results for $c_3 = 1$ (Case I), $c_3 = 2$ (Case II) and $c_3 = 3$ (Case III) are shown in figure 4. From figure 4(b), it is apparent that the qualitative shape of the spectrum is similar, and the only quantitative change is in the location of the maximum. The location of the maximum is shifting in accordance with the change in the mean particle size, which shifts to larger scale (smaller $k$) with increasing $c_3$. Moreover the logarithmic plot shown

in figure 4(c) indicates that the large $k$ tail for each of the cases is the same. The $-2$ spectrum is apparently unaffected by the asymmetry in the distribution.

To confirm the apparent weak dependence of the spectrum at large $k$ with the particle size distribution, a final test was done with an asymmetric case from above (Case I, $c_1 = 5$, $c_2 = 2$ and $c_3 = 2$), a Gaussian distribution (Case II) and the distribution of Case I inverted with respect to the particle size. The comparative results are shown in figure 5. Once again the curves are remarkably similar, with the exception of Case III which is beginning to show the oscillations present in narrower distributions. It appears that in this case the variance of the distribution as compared to the relatively large mean particle size is not sufficient to dampen the oscillations. Nevertheless the curves all appear to approach the $-2$ spectrum at large values of $\ln k$.

Having established that the density autocorrelation is relatively insensitive to the particle size distribution (aside from the scaling with the mean particle size, and so long as the distribution is sufficiently wide), we turn to the final parameter in the problem which is the particle concentration. As shown in Part I, the main effect of changing the particle concentration (all other parameters

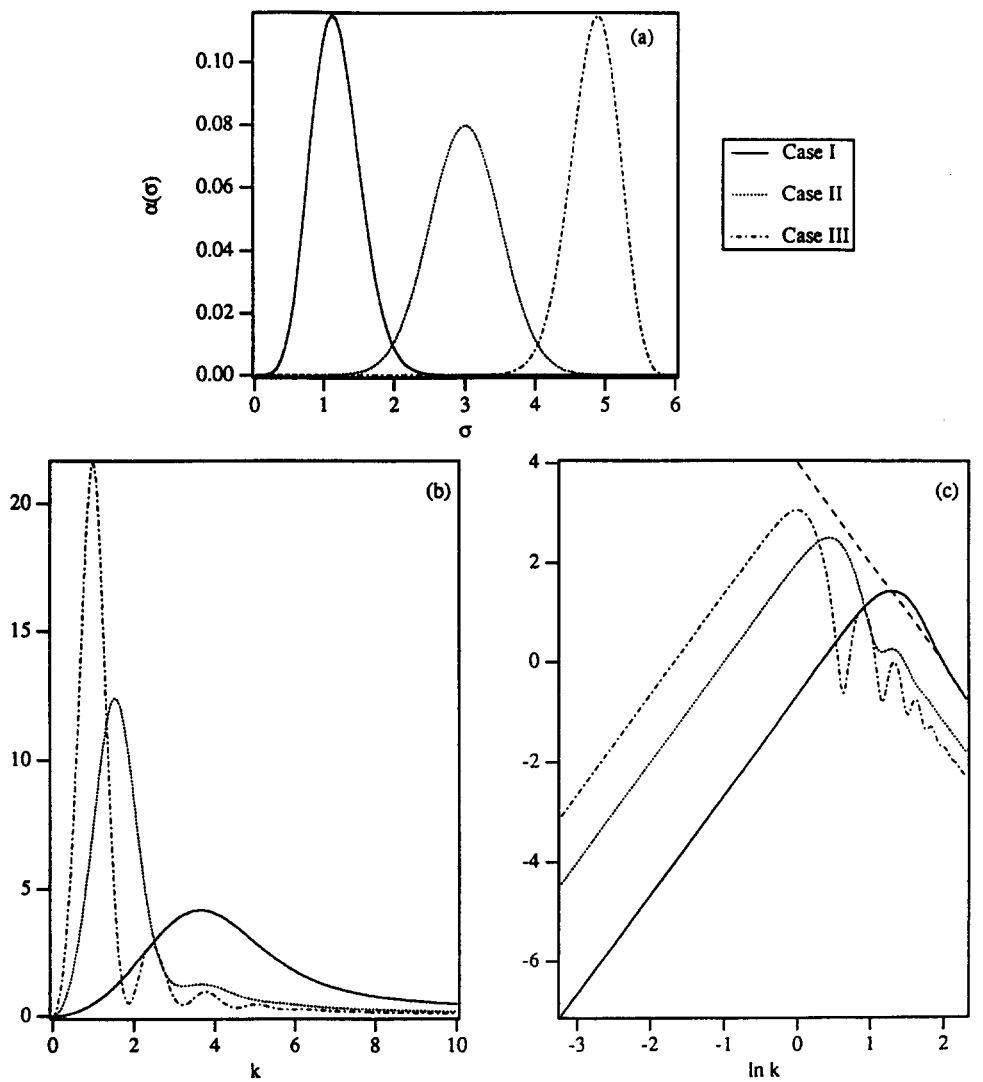


Figure 5. Effect of asymmetry of the particle size distribution on the density autocorrelation. Case I is a distribution described in [7] with $c_1 = 5$, $c_2 = 2$, $c_3 = 2$, Case II is a Gaussian (symmetric) and Case III is obtained by inverting Case II with respect to the particle size. Total particle concentration is maintained at 0.10. (a) Shows the particle size distributions, (b) shows the density autocorrelation in linear co-ordinates and (c) shows the same in logarithmic co-ordinates. The dashed line indicates a line of slope $-2$.

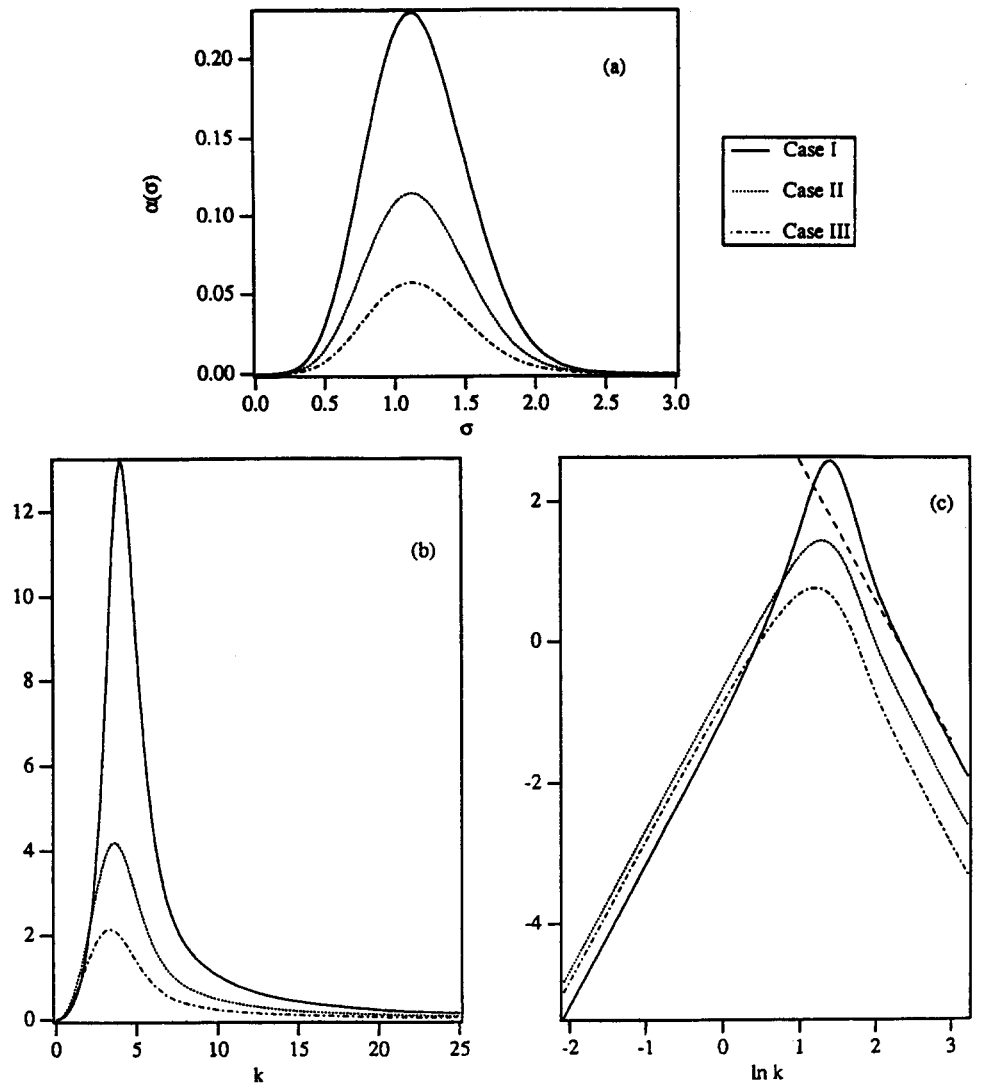


Figure 6. Effect of concentration on the density autocorrelation is observed by varying a particular distribution found from [7] ($c_1 = 5, c_2 = 2, c_3 = 2$) with respect to the total particle concentration. The concentrations are 0.20 (Case I), 0.10 (Case II) and 0.05 (Case III). (a) Shows the particle size distributions, (b) shows the density autocorrelation in linear co-ordinates and (c) shows the same in logarithmic co-ordinates. The dashed line indicates a line of slope −2.

being the same) is to change the mean separation distance. Mathematically we can approximate the mean separation distance by

$$\frac{\lambda}{\bar{\sigma}} \approx \left[\frac{2(1-\alpha_p)}{\alpha_p}\right]^{1/3}$$

where $\lambda$ is the mean separation distance, $\alpha_p$ is the total volume fraction of particles and $\bar{\sigma}$ is the volume averaged particle diameter. At low concentrations the mean particle size and the mean particle separation distance are widely disparate, however the influence of the mean separation distance is minimal because $\hat{h}_{ij}(k)$ and hence the density autocorrelation function is dominated by the geometric Overlap function $\hat{I}_{ij}(k)$. Conversely with increasing conentration the distribution functions become more important, however simultaneously the mean separation distance approaches the mean particle size. It therefore appears that the mean particle size is the dominant parameter and that the mean separation distance plays a minor role at all concentrations. This is demonstrated in figure 6, which shows a single particle distribution with decreasing particle

concentration. In each case the mean particle size is the same, and the curves appear to be essentially the same, aside from a scaling factor related to the integral constraint

$$\frac{1}{8\pi^3}\int B(\mathbf{k})\,d\mathbf{k} = \alpha_p\alpha_f$$

There appear to be two surprising results in this study. The first one is associated with the effect of polydispersity on the oscillations in the spectrum. The monodisperse system had multiple peaks associated with particle layers at ever increasing distances, however that coherency is lost in the polydisperse system, hence for sufficiently widely disperse systems the oscillations disappear completely. The second surprise is the relative insensitivity of the results to the exact nature of the particle size distribution. The only important parameter (aside from a normalization constant for $B$) is the mean particle size which determines the location of the maximum in the curve. Moreover the logarithmic plots at large $k$ implies a $-2$ spectrum for virtually all particle distributions, so long as they are sufficiently polydisperse that the oscillations are suppressed.

The -2 spectrum can be understood by re-considering the Overlap function. The previous study demonstrated at large $k$, $(\alpha_1/V_p)h(k) \ll 1$, hence the shape is dominated by the Overlap function. For a three-dimensional system of spheres, $\hat{I}_{ij}(k)$ given by [6] can be expanded to give

$$\hat{I}_{ij}(k) = \frac{4\pi^2\cos\left(\frac{k\sigma_i}{2}\right)\cos\left(\frac{k\sigma_j}{2}\right)\sigma_i\sigma_j}{k^4} - \frac{8\pi^2\cos\left(\frac{k\sigma_j}{2}\right)\sigma_j\sin\left(\frac{k\sigma_i}{2}\right)}{k^5} - \frac{8\pi^2\cos\left(\frac{k\sigma_i}{2}\right)\sigma_i\sin\left(\frac{k\sigma_j}{2}\right)}{k^5} + \frac{16\pi^2\sin\left(\frac{k\sigma_i}{2}\right)\sin\left(\frac{k\sigma_j}{2}\right)}{k^6}$$

At large $k$ the envelope for the oscillating $\hat{I}_{ij}(k)$ decays as $k^{-4}$, hence the envelope for the plots shown in figures 3–6 must decay as $k^{-2}$ because of the factor of $4\pi k^2$. In the polydisperse system, there is an $\hat{I}_{ij}(k)$ contribution for each particle size (as well as cross correlations), however they all decay as $k^{-4}$ at large $k$, therefore once the oscillations are eliminated by the interference of different phases, the curve decays monotonically like $k^{-4}$. Remarkably this result appears to be more closely tied to the shape of the particles than to their distribution.

This result has implications for multiphase flows of two immiscible fluids. For example consider Rayleigh–Taylor mixing, which occurs when a denser fluid is suspended above a lighter fluid in a gravitational field. For modeling purposes it may be tempting to conceptualize the mixing region as a collection of spheres of one fluid surrounded by the other. This simplistic thinking, however would not allow any other spectrum for the density autocorrelation than $-2$ as demonstrated above. Furthermore, if another spectrum existed within the mixing layer (e.g. $-5/3$) it would not imply that the size or spatial distribution of the blobs was incorrectly represented, but that their shape was not well represented by a sphere. Equivalently if real turbulence generates a spectrum different than $-2$ at large $\ln k$, the shapes of the individual regions must be something other than a sphere (unfortunately there are few measurements of the density spectrum in such a system, so we can only speculate).

## EXTENSION TO HIGHLY DRIVEN FLOWS

Once again, it is possible to extend the results presented in the previous section to the hypothetical flow caused by subjecting a particle–fluid mixture to an asymptotically large pressure gradient. The pressure gradient will cause the particulate phase to move relative to the fluid phase (i.e. interpenetration) as was seen in the monodisperse system, however in this case, though the velocity within a particular category will be uniform, the velocity of particles of different diameters need not be the same. This is evident by considering dependence of the terminal velocity of a particle on its diameter. It would appear that paticles with a larger diameter will achieve a greater terminal velocity than smaller ones. This introduces a fluctuational component to the particulate velocity even in this asymptotic limit. The particle velocities were estimated from their terminal

velocities. We consider both $\mathrm{Re} \to 0$ and $\mathrm{Re} \to \infty$ for the drag coefficient, resulting in the following relationships between the particle velocity and diameter

$$\mathrm{Re} \to 0: \quad \bar{\mathbf{u}}_j = \mathbf{U} \frac{\sigma_j}{\bar{\sigma}}$$

and

$$\mathrm{Re} \to \infty: \quad \bar{\mathbf{u}}_j = \mathbf{U} \sqrt{\frac{\sigma_j}{\bar{\sigma}}} \qquad [13]$$

where $\bar{\sigma}$ is the mean particle radius (see dimensional analysis above) and $\mathbf{U}$ is the velocity of the average size particle. The fluid velocity can then be expressed by (assuming the mean velocity is zero)

$$\bar{\mathbf{u}}_f = -\sum_{j=1}^{m} \frac{\alpha_j \bar{\mathbf{u}}_f}{\alpha_f} \qquad [14]$$

Equations [13] and [14] can be used to define the velocity fluctuation in terms of the $\beta$-correlations as shown below

$$\mathbf{u}'(\mathbf{x}) = \sum_{j=1}^{m} \beta_j(\mathbf{x})(|\bar{\mathbf{u}}_j - \bar{\mathbf{u}}_f|) \qquad [15]$$

Notice that the coefficient for each of the $\beta$-functions is no longer uniform because of the variations in the particle velocities. This introduces a complexity that was not seen in the monodisperse system because in that case, the particle diameters and the induced velocities were constant. The effect this has on higher-order moments can be seen by considering the turbulent mass flux, which is defined as $\mathbf{A} = \overline{\rho'(\mathbf{x})\mathbf{u}'(\mathbf{x}+\mathbf{r})}$. From [7] and [15] we have

$$\mathbf{A}(\mathbf{r}) = (\rho_p - \rho_f) \sum_{j=1}^{m} (|\bar{\mathbf{u}}_j - \bar{\mathbf{u}}_f|) \sum_{i=1}^{m} \beta_{ij}(\mathbf{r}) \qquad [16]$$

It is clear from [16] that the spectral shape of the mass flux will differ from the density autocorrelation because the particle velocities introduces a weighting factor into the sum over the $\beta$-correlations. Figure 7 shows a normalized plot of $\hat{B}(k)$ and $\hat{\mathbf{A}}(k)$ for a Gaussian particle size distribution, and with the two different dependencies of the particle velocity with diameter (see [13]). The weighting favors the large-scale contributions over the small scale ones, therefore the $\hat{\mathbf{A}}(k)$ curve appears to be shifted toward small $k$ (large scale). This is even more apparent in figure 8, which shows a comparison between $\hat{B}(k)$ and the normalized, non-zero component of the Reynolds stress $\hat{\underline{\underline{\mathbf{T}}}}(k)$. Because the Reynolds stress is second order in velocity the shift is more dramatic.

It was shown in Part I that for a monodisperse system of particles, the spectra of virtually all moments coincide with the B-spectrum in this asymptotic limit. This is not the case for a polydisperse system, however, because the weighting of the $\beta$-correlations depends on the order in velocity of the higher-order moment. This implies spectra *of a given order in velocity* will collapse, but not necessarily correlations that have different orders in velocity. This severely complicates the results shown previously in table 1 of Part I because there is no longer a simple relationship between the higher-order moments and the select variables [$\bar{\rho}$, $b$, $\mathbf{A}$ and $B(\mathbf{r})$]. For completeness we tabulate the same moments for the polydisperse system minus column 3 which is no longer relevant.

Part I also included a perturbation analysis for estimasting the effect that hydrodynamic forces may have on the interpenetrating particles. The hydrodynamic attractive potential was caused by a Bernoulli force that acts in the direction of the separation vector between the particles. An equivalent force will also be acting on the polydisperse particles, however the analysis would no longer be valid because effects due to relative motion of particles of different sizes may overwhelm the venturi force. We therefore defer the discussion of the instability of the particle assembly until a more realistic direct numerical simulation or experiment can provide the necessary information.

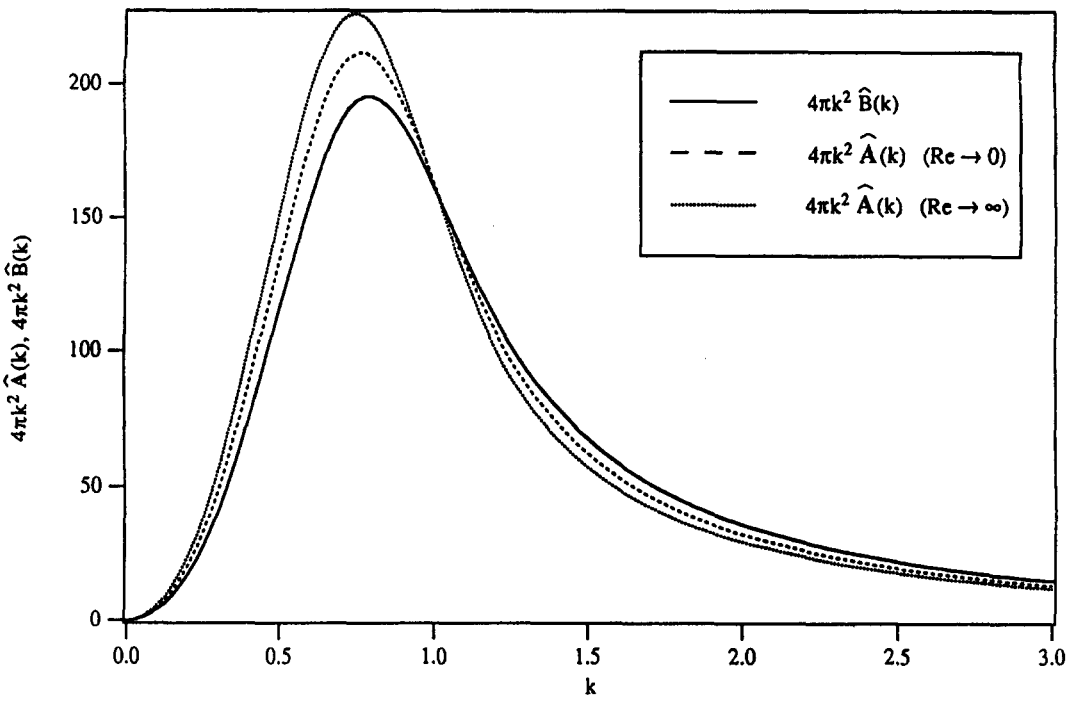


Figure 7. A normalized plot of $4\pi k^2\hat{A}(k)$ with two limiting velocity dependencies ([13]) and a Gaussian particle size distribution. A plot of $4\pi k^2\hat{B}(k)$ is also shown for the sake of comparison.

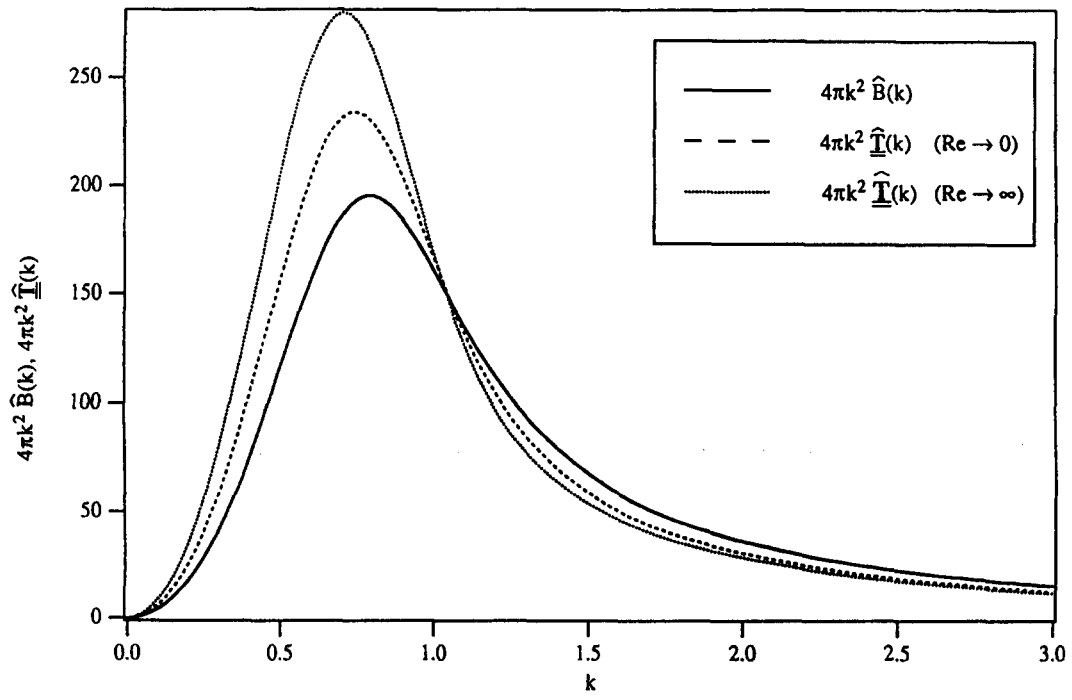


Figure 8. A normalized plot of the non-zero component of $4\pi k^2\hat{\underline{\underline{T}}}(k)$ with the two limiting velocity dependencies ([13]) and a Gaussian particle size distribution. Again, a plot of $4\pi k^2\hat{B}(k)$ is also shown for the sake of comparison.

Table 1. Relationships for several common higher-order spectral moments in terms of the $\beta_{ij}$ correlations for the ideal case of uniform interpenetration of the particulate and fluid phases. Note that terms shown in brackets in column 1 are evaluated at the same point and tensors have been designated by a "=" subscript

| High-order moment | Relationship to $\beta$-correlation |
|---|---|
| (1) $B(\mathbf{r}) = \overline{\rho'\rho'}$ | $(\rho_p - \rho_f)^2 \sum_{i=1}^{m}\sum_{j=1}^{m} \beta_{ij}$ |
| (2) $b(\mathbf{r}) = -\overline{\rho'\left(\frac{1}{\rho}\right)'}$ | $\frac{(\rho_p - \rho_f)^2}{\rho_p\rho_f} \sum_{i=1}^{m}\sum_{j=1}^{m} \beta_{ij}$ |
| (3) $\mathbf{A}(\mathbf{r}) = -\overline{\rho'\mathbf{u}'}$ | $(\rho_p - \rho_f) \sum_{i=1}^{m}\sum_{j=1}^{m} \beta_{ij}(\bar{\mathbf{u}}_j - \bar{\mathbf{u}}_f)$ |
| (4) $\overline{\rho'(\mathbf{u}'\rho')}$ | $(\alpha_p - \alpha_f)(\rho_p - \rho_f)^2 \sum_{i=1}^{m}\sum_{j=1}^{m} \beta_{ij}(\bar{\mathbf{u}}_j - \bar{\mathbf{u}}_f)$ |
| (5) $\overline{\frac{1}{\rho}\mathbf{u}'}$ | $\frac{(\rho_p - \rho_f)}{\rho_p\rho_f} \sum_{i=1}^{m}\sum_{j=1}^{m} \beta_{ij}(\bar{\mathbf{u}}_j - \bar{\mathbf{u}}_f)$ |
| (6) $\overline{(\rho C_p \mathbf{u}'')T''}$ | $\frac{\rho_p C_p T_p(\rho_p - \rho_f)}{\alpha_p\rho_p + \alpha_f\rho_f} \sum_{i=1}^{m}\sum_{j=1}^{m} \beta_{ij}(\bar{\mathbf{u}}_j - \bar{\mathbf{u}}_f)$ |
| (7) $\underline{\mathbf{R}}(\mathbf{r}) = \overline{(\rho\mathbf{u}'')\mathbf{u}''}$ | $\frac{\rho_p\rho_f \sum_{j=1}^{m}\sum_{j=1}^{m} \beta_{ij}(\bar{\mathbf{u}}_i - \bar{\mathbf{u}}_f)(\bar{\mathbf{u}}_j - \bar{\mathbf{u}}_f)}{\alpha_p\rho_p + \alpha_f\rho_f}$ |
| (8) $\underline{\mathbf{T}}(\mathbf{r}) = \overline{\mathbf{u}'\mathbf{u}'}$ | $\sum_{i=1}^{m}\sum_{j=1}^{m} \beta_{ij}(\bar{\mathbf{u}}_i - \bar{\mathbf{u}}_f)(\bar{\mathbf{u}}_j - \bar{\mathbf{u}}_f)$ |

## CONCLUSIONS

Previous calculations of the spectrum of the density autocorrelation for a monodisperse particle–fluid system have been extended to the more general case of a polydisperse system with a wide range of particle sizes. It was observed that, with an increasing width of the particle size distribution or polydispersity, the oscillations in the autocorrelation curve were dampened or even eliminated in certain cases, leading to a smooth, monotonically decreasing curve at large $k$. Furthermore at large wavenumbers the autocorrelation was found to obey a $-2$ power-law spectrum dictated by the spherical geometry assumed in the problem. These results are general and the autocorrelation does not seem to be sensitive to any variations in the exact nature of the size distribution or the particle concentration, so long as the distribution is sufficiently wide. The fact that the autocorrelation spectrum is locked into a $-2$ spectrum at large wavenumbers implies a limitation in the use of the analogy between variable-density and multiphase flows, proposed by Collins (1992) at the spectral level. This limitation can be overcome by relaxing the restriction of the present study of spheres to more general particulate flows. That work is in progress.

The results for the density autocorrelation were extended to the special case of a particle–fluid system experiencing an asymptotically large pressure gradient. Again it was shown that higher-order moments can be calculated from the $\beta$-correlations, however in this case the particle velocities provide a weighting of the functions that depends on the order in velocity of the moment. It appears that collapse of spectra of a given order in velocity is observed, but spectra of different orders in velocity are unique. They can be characterized by the functional relationship between the particle velocity and particle size for which two examples were given ($\mathrm{Re} \to 0$, $\mathrm{Re} \to \infty$). The simple relationships that reduced the order in the monodisperse particle system are lost in the polydisperse case. Furthermore the analysis for determining the effect of the induced hydrodynamic force on the particles could not be extended because it appears that other effects may dominate (e.g. relative motion of particles of different size). A thorough understanding of the effect of polydispersity on quantities such as the RDF and other two-point correlations required in the theory presented herein will come from experimental and simulation data. Work along these lines is in progress.

*Acknowledgement*—The authors wish to acknowledge support for this study from Dow Chemical through the Young Minority Investigator Award (awarded to L. R. Collins).

## REFERENCES

COLLINS, L. R. 1992 Closure approximations for the Reynolds stress transport equation for variable-density turbulence. *Proceedings of the 13th Int. Symposium on Turbulence*, University of Missouri-Rolla.

ISHII, M. 1975 *Thermo-fluid Dynamic Theory of Two Phase Flow*. Eyrolles, Paris, France.

LEBOWITZ, J. L. 1964 Exact solution of generalized Percus–Yevick equation for a mixture of hard spheres. *Phys. Rev.* **133,** A895–899.

PERCUS, J. K. & YEVICK, G. J. 1958 Analysis of classical statistical mechanics by means of collective coordinates. *Phys. Rev.* **110,** 1–13.

SMITH ,W. R. & HENDERSON, D. 1970 Analytical representation of the Percus–Yevick equation for Lennard–Jones and hard-sphere potentials. *Molec. Phys.* **19,** A411–415.

SUNDARAM, S. & COLLINS, L. R. 1994 Spectrum of density fluctuations in a particle–fluid system—I. Monodisperse spheres. *Int. J. Multiphase Flow* **20,** 1021–1037.